Food Chemistry: X 13 (2022) 100194

Contents lists available at ScienceDirect

Food Chemistry: X

journal homepage: www.sciencedirect.com/journal/food-chemistry-x

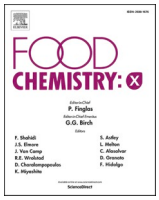

Studies into interactions and interfacial characteristics between cellulose nanocrystals and bovine serum albumin

Xinna Hu [a,b,c], Tao Ma [a,b,c], Shuyu Lu [a,b,c], Yi Song [a,b,c,*]

[a] College of Food Science and Nutritional Engineering, China Agricultural University, Beijing 100083, China
[b] National Engineering Research Center for Fruits and Vegetable Processing, Beijing 100193, China
[c] Key Laboratory of Fruits and Vegetable Processing, Ministry of Agriculture and Rural Affairs, Beijing 100083, China

ARTICLE INFO

Keywords:
Cellulosic material
Bovine serum albumin
Electrostatic complex

ABSTRACT

This study investigates the interactions between cellulose nanocrystals (CNCs) and bovine serum albumin (BSA) under different pH conditions. A multiscale technique was employed to characterize the CNCs and BSA at pH 7 and pH 3. ζ-Potential measurement and UV–vis spectroscopy demonstrated strong interactions between CNCs and BSA at pH 3, whereat they have opposite charges. Interfacial tensiometry showed a deficiency in the surface activity of the CNCs and indicated that BSA dominated the interface behavior in their complex. Quartz crystal microbalance with dissipation revealed that the sequential adsorption of BSA and CNCs produced viscoelastic bilayers at pH 3, and the mass adsorbed was ~ 28 times that adsorbed at pH 7. Molecular dynamics simulations indicated that the key interactions between the two materials were produced between the hydrophobic CNC surface and the BSA domain IIA region. These results provide interesting insights into the design of complex food emulsions and fluid interfaces.

1. Introduction

In the past few decades, protein/polysaccharide interactions have gained extensive attention owing to their great importance in the fields of food and chemical engineering. They are commonly utilized in the development of colloidal structures (such as emulsions and foams) that exhibit diverse properties based on their excellent surface activities (Wijaya, Patel, Setiowati, & Van der Meeren, 2017). It has also been demonstrated that the resistance of protein-stabilized colloidal systems to various environmental stresses (such as pH, thermal processing, and ionic strength) can be improved by the sequential introduction of a polysaccharide layer, which is known as layer-by-layer assembly (Richardson et al., 2016). Typically, to build protein/polysaccharide-coated colloidal structures, a protein-coated droplet must be initially prepared, followed by successive interfacial complexation by the introduction of oppositely charged polysaccharides (Li, McClements, Liu, & Liu, 2020). The interfacial complexation between proteins and polysaccharides is primarily driven by electrostatic attractions, and sometimes involves hydrogen bond formation or hydrophobic interactions (Li et al., 2019). Among the various environmental factors affecting interfacial complexation, pH is considered to be the most important because it determines the charges of biological macromolecules and, thus, could alter the strength of the electrostatic interactions (Pathak, Priyadarshini, Rawat, & Bohidar, 2017). Such interactions can be either repulsive or attractive and are determined mainly by the charges of the proteins and polysaccharides. From this perspective, it is of great significance to gain a deeper understanding of the effect of pH on the interfacial complexation of these species to ultimately offer insights into the elaborate structural design of complex emulsions.

Cellulose nanocrystals (CNCs) are emerging nanomaterials that have been isolated from plants *via* acid hydrolysis. They have received widespread attention in recent years because of their high specific surface areas, nontoxic nature, sustainability, biocompatibility, and biodegradability (Ma et al., 2020). The unique rod-like structures of CNCs endows them with a strong steric barrier, and the sulfuric half-ester groups ($-OSO_3^-$) introduce many negative charges on the CNC surfaces (Sarkar, Zhang, Holmes, & Ettelaie, 2019). Some studies have reported the combination of CNCs and surface-active proteins in emulsions, such as whey protein isolate (Sarkar, Li, Cray, & Boxall, 2018), sodium caseinate (Urbánková, Sedláček, Kašpárková, & Bordes, 2021),

Abbreviations: CNCs, cellulose nanocrystals; BSA, bovine serum albumin; QCM-D, quartz crystal microbalance with dissipation; TEM, transmission electron microscopy; MD, molecular dynamics.

* Corresponding author at: College of Food Science and Nutritional Engineering, China Agricultural University, Beijing 100083, China.
E-mail address: sy587@hotmail.com (Y. Song).

https://doi.org/10.1016/j.fochx.2021.100194
Received 3 November 2021; Received in revised form 20 December 2021; Accepted 21 December 2021
Available online 22 December 2021

and zein (Wei et al., 2021). These studies mainly focused on evaluation of the emulsion performances based on their stabilization by CNC–protein complexes; however, there is currently a relatively limited understanding of the interactions between rod-like CNC particles and proteins. Thus, a better understanding of CNC–protein interactions is vital for the design and development of food products exhibiting functional properties. Bovine serum albumin (BSA) is a commercially available and well-understood protein with approximate dimensions of 4 × 4 × 14 nm (Peters, 1995). BSA has higher surface-active properties than other proteins (such as soy proteins, ovalbumin, β-casein, and β-lactoglobulin), and has been widely utilized in both food and pharmaceutical systems (Liu, Zheng, Huang, Tang, & Ou, 2018). Therefore, BSA was selected as a representative globular protein for the purpose of this study because it serves as a good model for studying CNC–protein interactions.

In this work, our study begins by examining the surface and interface activities of CNCs and BSA in solution, wherefor combinational techniques, including UV–vis spectroscopy and tensiometry, are conducted to characterize the interactions in the bulk phase. Subsequently, the real-time sequential adsorption of CNCs and BSA at the interface and the influence of pH on the interactions between the two species are investigated using the quartz crystal microbalance with dissipation (QCM-D) technique. QCM-D has attracted considerable attention as a facile and effective tool for investigating molecular adsorption onto a solid surface. Compared with labor-intensive and time-consuming chemical analytical techniques, it provides not only quantitative information at the nanogram scale but also realizes real-time monitoring (Chen, Xu, Liu, Masliyah, & Xu, 2016). Detailed information regarding the interfacial layer (such as its adsorption/desorption properties, thickness, and viscoelasticity) can also be obtained using the QCM-D technique (Lee et al., 2017). Recently, QCM-D technique has been widely used to examine the interactions between nanoparticles bearing functionalized surfaces in aqueous solutions, in addition to the adsorption kinetics of polymers and proteins (Chen et al., 2016). These studies confirmed that the QCM-D technique is highly suitable for exploring the interactions between proteins and polysaccharides at the interface. Finally, we examine the binding mode of CNCs with BSA by employing molecular dynamic simulations to increase our knowledge on the interactions of CNCs with this protein at the molecular level.

2. Materials and methods

2.1. Materials

CNCs hydrolyzed by sulfuric acid were obtained from CelluForce Inc. (Montreal, Canada), 12.5 of sulfate ester groups per 100 anhydro glucose units. BSA (96% purity) was purchased from Sigma-Aldrich (St Louis, MO, USA). Corn oil was purchased from a local supermarket. The phosphotungstic acid negative staining solution was purchased from Solarbio Technology Co., Ltd. (Beijing, China). Other chemicals used were of analytical grade and purchased from Aladdin Biochemical Technology Co., Ltd. (Shanghai, China). Ultrapure water (18 MΩ·cm) was used throughout the experiments.

2.2. Preparation of the CNC and BSA dispersions

The BSA solutions were obtained by dissolving BSA powder in water and stirring continuously for 4 h using a magnetic stirrer (JJ-1H, Changzhou Maikenuo Instruments Co., Ltd., Jiangsu Province, China). The CNCs were added to the water and stirred for 4 h and then sonicated at 30% amplitued for 3 min (3 s on, 2 s off) using a Probe Sonicator (SCIENTZ-IID, Ningbo Scientz Biotechnology, China).

2.3. Transmission electron microscopy (TEM)

The surface morphology of the CNCs was observed *via* TEM (JEM 2100F, JOEL Japan Electronics Co., Ltd., Tokyo, Japan) with an acceleration voltage of 60 keV. Prior to the examination, one drop of the 0.1 wt% CNC suspension was deposited on a copper grid immediately after sonication and dried for 60 min at 25 °C. The grid was then gently blotted with filter paper to remove any excess droplets. Subsequently, the samples were negatively stained with phosphotungstic acid (2 wt%) and observed by TEM after air-drying. The particle dimensions were determined by measuring 50 individual nanocrystals using ImageJ software.

2.4. ζ-potential

The ζ-potential of CNC suspension and BSA solutions at pH 1–7 was determined using a Zetasizer Nano instrument (ZS90, Malvern, UK).

2.5. Visual assessment of CNC/BSA interactions

To visually assess the CNC/BSA interactions at different pH values, the 1.0 wt% CNC suspension and the 1.0 wt% BSA solution were adjusted to pH 3 or pH 7 by adding HCl or NaOH (0.1 mol/L), respectively. Subsequently, the CNC and BSA dispersions were mixed at different mass ratios of 10:1, 5:1, 2:1, and 1:1 of CNC: BSA, and then vortexed.

2.6. Fourier transform infrared (FT-IR) spectroscopy

The structural properties of CNCs, BSA and their mixtures were analyzed by FT-IR with the PerkinElmer Spectrum 100 instrument (Perkin Elmer, Waltham, MA, USA). The data were recorded over the range from 4000 to 400 cm^{-1}, with a resolution of 4 cm^{-1}.

2.7. Transmittance measurements

The transmittances of the CNC/BSA mixtures were assessed by UV–vis spectroscopy using an ultramicro spectrophotometer (Thermo Scientific, USA). The testing wavelength covered a broad range of 300–800 nm.

2.8. Surface and interfacial tension measurements

The surface and interfacial tensions were determined *via* the pendant drop method using a contact angle measuring instrument (OCA25, Dataphysics Instruments GmbH, Filderstadt, Germany). A 1.65 mm stainless steel needle was used to form the droplet for surface tension analysis and a 0.91 mm needle was employed for interfacial tension analysis. The droplet image was captured and analyzed 10 min after the critical state of the droplet was formed. The tension was determined by fitting the shape of the droplet and by calculation using the Young–Laplace equation. The following samples were tested at both pH 3 and pH 7. (a) The individual CNC and BSA suspensions at concentrations of 0.01–1.0 wt%; (b) a 1.0 wt% CNC suspension with BSA added at concentrations ranging from 0.2 to 1.0 wt%; and a 1.0 wt% BSA solution with CNC added at concentrations ranging from 0.2 to 1.0 wt%. All experiments were performed at both the air/water and oil/water interfaces.

2.9. QCM-D analysis

2.9.1. QCM-D experiments

A SiO_2 sensor (QSX 303) with a fundamental frequency of 4.95 MHz was selected for QCM-D analysis. Before each experiment, a thorough pre-cleaning protocol was used to ensure reproducible results. Briefly, the sensor was first immersed in 2.0 wt% Hellmanex (Hellma GmbH, Müllheim, Germany) for 30 min and then plasma-treated for 10 min. The sensor was then rinsed repeatedly with ethanol and Milli-Q water, and fully dried with nitrogen gas.

The adsorption features of the CNCs and BSA and their interaction performances were investigated using a QCM-D apparatus (Q-Sense E4, Biolin Scientific, Gothenburg, Sweden). Before commencing, the system was thoroughly cleaned with 2.0 wt% Hellmanex and then rinsed with Milli-Q water. The system was then purged successively with air and ultrapure water to achieve a stable baseline. Prior to data collection, each test began with pre-equilibration in the adjusted buffer at the desired pH for 10 min. The sample was then pumped until a steady frequency and dissipation were reached. Each test ended with a final rinse to remove any loosely attached components.

To explore the properties of monolayer adsorption, 1.0 wt% BSA solutions at pH 3 and pH 7 were measured individually. Each sample was pumped into the chamber until a stable frequency and dissipation were reached. Subsequently, a rinsing step was conducted with the adjusted buffer to remove any loose components. Sequential adsorption was then studied by successive addition of the 1.0 wt% BSA solution and the 1.0 wt% CNC dispersion. All poorly adsorbed components were removed by immediate rinsing after each adsorption stage. Sequential adsorption was investigated at pH 3 and pH 7. All tests were performed at 25 °C with a flow rate of 0.1 mL/min.

2.9.2. QCM-D data analysis

The frequency shift (Δf) and change in dissipation (ΔD) were monitored at several overtones in all QCM-D experiments. Data analysis was performed using the QTools software (Biolin Scientific). In the simplest case, where a thin, evenly distributed, and rigid adsorbed layer is assumed, the relationship between the frequency shift and the mass adsorbed (Δm; ng/cm^2) can be described by the Sauerbrey model (Sauerbrey, 1959), as given in Eq. (1):

$$\Delta m = -\frac{C}{n}\Delta f \tag{1}$$

where C is the fundamental resonance frequency (17.7 ng/cm^2/Hz for a 4.95 MHz crystal) and n is the overtone number (n = 1, 3, 5…,13). The data at the 5th overtone were selected to estimate the adsorbed mass. It is worth noting that the Sauerbrey model is applied to rigid layers, while the Voight model is commonly used for viscoelastic films (Lozeau, Rolle, & Camesano, 2018). However, many recent studies have indicated that it is unreasonable to apply the Voight model to investigate monolayers of globular proteins or any other discrete nanoscale particles because of the lateral heterogeneity of the film (Li, Wu, Doost, Su, & Van der Meeren, 2021). This research focuses on semi-quantitative analysis and is sufficiently convincing to characterize the interfacial interactions between the CNCs and BSA using the traditional Sauerbrey model.

2.10. Molecular dynamics (MD) simulations

All-atom simulations were conducted using the GROMACS software package (Van Der Spoel et al., 2005). Simulation snapshots were generated using the Visual Molecular Dynamics (VMD) software package. The CNCs used in this study correspond to the I_β crystal structure, which is the most common cellulose arrangement in higher plants. The crystal structure of the CNCs (with ~ 4 nm diameter and ~ 11 nm length, 15,228 atoms) was constructed using a cellulose builder toolkit with the CHARMM36 carbohydrate force field (Gomes & Skaf, 2012). The CNCs possess a hexagonal cross-section and consist of 36 chains. The structure of BSA was obtained from the Protein Data Bank (PDB code: 4F5S; https://www.rcsb.org/). The BSA and CNC molecules were placed in a rectangular periodic box (15.0 × 15.0 × 15.0 nm^3) filled with TIP3P water models. K^+ was chosen as the counterion to neutralize the system. After an initial energy minimization of the system, a 250 ps NVT ensemble (number, volume, and temperature) simulation for equilibration was conducted with a time step of 1 fs. The temperature was maintained at 298.0 K using the Nose-Hoover thermostat with a time constant of 1 ps. A 100 ns NPT (number, pressure, and temperature) simulation was then performed with a time step of 2 fs and using the same temperature coupling as that employed in the NVT simulation. The pressure of the system was equilibrated at 0.1 MPa using a Parrinello-Rahman barostat coupled with a time constant of 5 ps. The minimum distance was recorded using the GROMACS gmx mindist tool.

2.11. Data analysis

All experiments were performed at least in triplicate. Data were manipulated by analysis of variance (one-way ANOVA) using SPSS software (SPSS Inc., Chicago, IL). Differences were determined using Tukey's test and considered significant at $p < 0.05$.

3. Results and discussion

3.1. Characterization of CNCs

The TEM image showed that the CNCs had a typical rod-like shape with a width of 6.2 ± 1.5 nm and a length of 133.6 ± 28.7 nm (Fig. S1). In addition, Fig. S2a shows that the CNCs were negatively charged in the selected pH range (pH 1–7). This negative charge originates from the grafting of negatively charged sulfate half-ester groups (–OSO_3^-) during sulfuric acid hydrolysis (Sarkar et al., 2019). It can also be seen from this figure that the ζ-potential is susceptible to the pH. More specifically, the ζ-potential gradually decreased from a high absolute value of 58.9 mV at pH 7 to an absolute value of 14.2 mV at pH 1. This was attributed to protonation of the CNC surface groups under acidic conditions (Mikulcová, Bordes, Minařík, & Kašpárková, 2018).

According to the literature, the isoelectric point (pI) of BSA is 4.7 (Peters, 1995). As shown in Fig. S2b, the net charge of BSA is dependent on the pH, wherein reducing the pH below the pI leads to the protonation of the BSA functional groups, resulting in an overall positive charge. Conversely, BSA is negatively charged when the pH level is above the pI. Thus, pH 3 and pH 7 were selected as representative values to investigate the interactions between the CNCs and BSA, which have the opposite charge at pH 3 and the same charge at pH 7. It was therefore expected that the control of the electrostatic interactions between the CNCs and BSA could be achieved by simply regulating the pH of the aqueous phase.

3.2. Bulk studies of CNCs and BSA dispersions

The interactions between the CNC and BSA mixtures at pH 3 and pH 7 were investigated by visual observations, transmittance measurements, and ζ-potential measurements at different CNC/BSA mass ratios (i.e., 10:1, 5:1, 2:1, and 1:1). At pH 7, the CNC/BSA mixtures were negatively charged (Fig. 1b), and so no visible changes were observed (Fig. 1a). The UV–vis spectroscopy results also showed that the four mixed suspensions were all transparent at pH 7, with a transmittance > 95% being recorded at 600 nm (Fig. 1c). However, it was observed that the transmittance of the mixtures increased with a decrease in the proportion of CNCs. This was attributed to the fact that the CNC suspension was light blue in color, while the pure BSA solution was colorless and transparent in appearance. Therefore, lower proportions of CNCs in the mixtures resulted in a reduced turbidity and a higher transmittance. At pH 3, the CNC/BSA mixtures formed a turbid gel at all CNC/BSA ratios ranging from 10:1 to 1:1 (Fig. 1a). As above, the transmittance increased with a decrease in the CNC proportion, and compared to the observations at pH 7, the transmittance of all mixtures was significantly reduced over all regions between 300 and 800 nm (Fig. 1d) because the two polymers were oppositely charged at this pH value. As a result, strong electrostatic interactions led to the formation of CNC/BSA complexes, as evidenced by both the above-mentioned decrease in transmittance and the change from negative to positive in ζ-potential.

The FT-IR spectrums of CNCs, BSA and their complex at different pH are shown in Fig. S3. There exist several similar peaks in CNCs and BSA

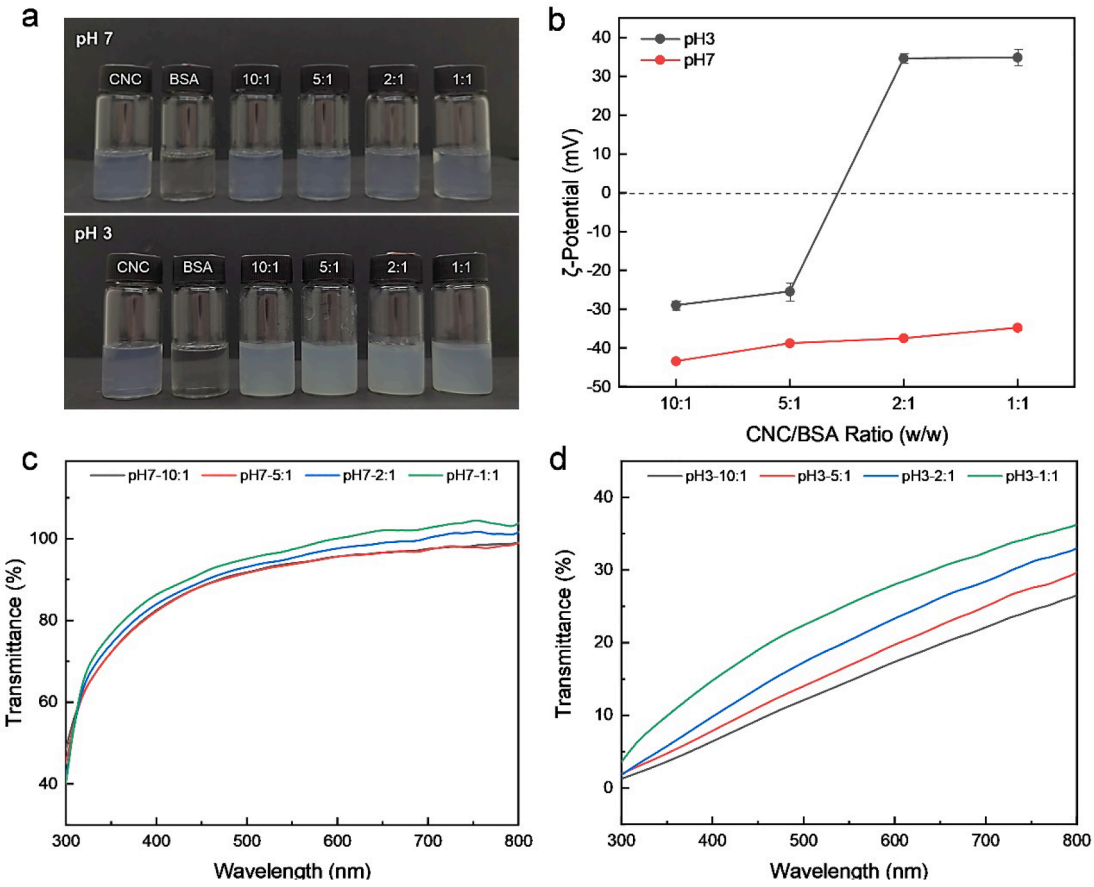

Fig. 1. Characterizations of CNC/BSA mixtures. (a) Visual appearance, (b) ζ-potential, (c) and (d) transmittance of CNC/BSA mixtures at different mixing ratio (10:1, 5:1, 2:1, 1:1. w/w) at pH 3 and pH 7, respectively.

due to a certain degree of similarity in their molecular structure. Individual BSA and CNCs spectra both display broadband between 3600 and 3100 cm^{-1} that originating from –NH stretching vibrations of BSA and –OH stretching vibrations of CNCs, respectively. The peak at 2900 cm^{-1} was assigned to the C—H stretching vibration of CNCs. The absorption bands of BSA between 1700 and 1500 cm^{-1} originate from carbonyl stretching vibrations (Amide I) and NH bending vibrations (Amide II). The biggest difference between CNCs and BSA was found at 1535 cm^{-1}, where BSA exhibited carbonyl and N—H variable angle vibration while CNCs didn't (Liu et al., 2018). Compared with peak in pure BSA (3314 cm^{-1}), the corresponding peak in CNC/BSA mixtures apparently shifted towards higher wavenumbers (3342 cm^{-1} for CNC/BSA-pH7 and 3348 cm^{-1} for CNC/BSA-pH3). This shift indicates the formation of intermolecular bonds, such as electrostatic interactions, which could shorten the bond length of the –NH functional groups, thus increasing the wavenumber (Derkach, Voron'ko, Sokolan, Kolotova, & Kuchina, 2020).

3.3. Surface and interfacial activities

3.3.1. Individual CNC and BSA dispersions

Insight into the interfacial properties of CNCs and BSA is fundamentally important for further analysis of their interactions. Thus, we initially investigated the surface and interfacial activities of individual CNC dispersion and BSA solution at pH 3 and pH 7, with the purpose of evaluating their ability to compete at the interface. This test covered a broad concentration range from 0.01 to 1.00 wt%, and the results are presented in Fig. 2. At the air/water interface at pH 7 (Fig. 2a), the surface tension of the CNC dispersion did not change as the concentration increased in a short time scale, which stabilized at ~ 73 mN/m. This indicated that CNCs is insufficient to reduce surface tension in the short time. However, it's important to note that CNCs do reduce the surface tension when employing the Wilhelmy-Plate Technique and monitoring in a longer time scale (15 h), as reported by Bertsch et al. (2018). The BSA solution presented good surface activity and effectively reduced the surface tension at a concentration > 0.5 wt%, which indicated the strong adsorption of BSA molecules at the air/water interface. Upon increasing the concentration of BSA to 1.0 wt%, the surface tension decreased from 72.8 to 64.5 mN/m. This dependence of the surface tension on the protein concentration has also been reported in previous studies (Nguyen, Waton, Vandamme, & Krafft, 2013). Furthermore, when the pH was reduced to 3 (Fig. 2b), the BSA solution exhibited a superior surface activity, and the surface tension further decreased to 53.1 mN/m at 1.0 wt% BSA. The surface tension of the CNC dispersion exhibited a trend similar to that observed at pH 7, indicating that lowering the pH has a limited effect on the air/water surface activity of the CNCs.

In terms of the oil/water interface at pH 7 (Fig. 2c), the CNC dispersion did not exhibit interfacial activity under a short time and present concentration conditions, which may be due to its inherent negative charge at this interface (Liu et al., 2017). However, similar as the surface tension, it is important to note that CNCs do reduce the interfacial tension when employing the pendant drop method but monitoring in a longer time scale (Bergfreund, Sun, Fischer, & Bertsch, 2019). In contrast, the interfacial tension of the BSA solution decreased rapidly from 21.8 to 19.4 mN/m upon increasing the BSA concentration from 0.01 to 0.2 wt% although a further increase to 1.0 wt% BSA had a negligible effect on the oil/water interfacial tension. At pH 3, different trends were observed at the oil/water interface (Fig. 2d). More specifically, the CNC dispersion exhibited a good interfacial activity at pH 3, with a slight decrease in the interfacial tension being observed compared to that at pH 7. In this acidic environment, the assembly of

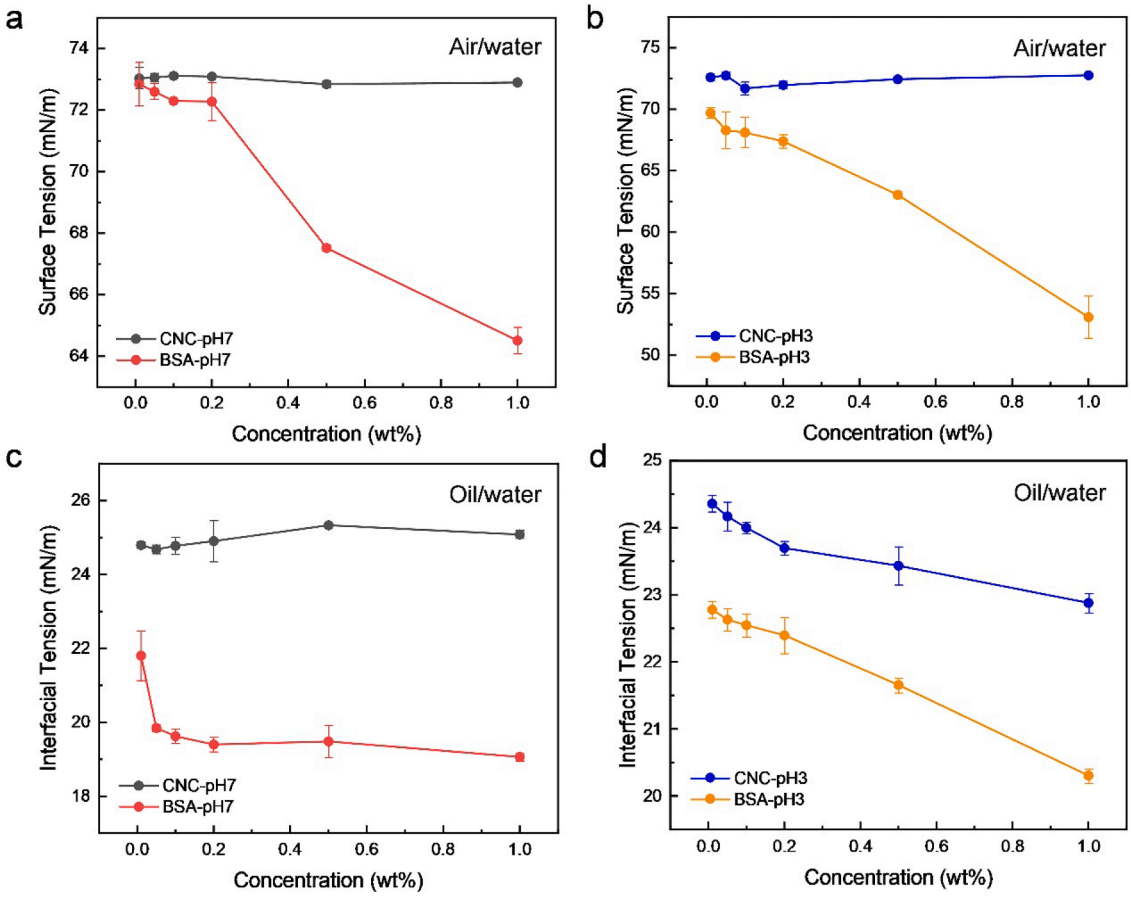

Fig. 2. Surface and interfacial activities of CNC and BSA individuals. (a) Surface tension at pH 7, (b) Surface tension at pH 3, (c) Interfacial tension at pH 7, (d) Interfacial tension at pH 3.

CNCs due to the loss of electrostatic repulsion may increase their areal density, thereby leading to a reduction in the interfacial tension (Wu et al., 2019). Furthermore, the interfacial tension of BSA decreased linearly with the increase in concentration, and the final value at a concentration of 1.0 wt% was similar to that obtained at pH 7.

3.3.2. *CNC/BSA mixtures*

The surface and interfacial tensions of the CNC/BSA mixtures were then tested to evaluate their ability to compete at the interface. The mixed systems were prepared using BSA or CNC concentrations of 1.0 wt % and then adding the corresponding CNC suspension or BSA solution as desired. At pH 7 (Fig. 3a), no significant changes in the air/water surface tension were observed upon increasing the concentration of the CNCs in the BSA solution because of the repulsion between the CNCs and BSA, in addition to the lack of surface activity exhibited by the CNCs. A similar trend was observed for the oil/water interfacial tension, thereby indicating that the CNCs played no dominant role in determining the interfacial activities of the CNC/BSA mixtures. On the other hand, upon increasing the BSA concentration in the CNC suspension, the air/water surface tension decreased from 71.6 to 68.2 mN/m, and the oil/water interfacial tension decreased from 18.9 to 15.7 mN/m. This indicates that in a mixed system, the most surface-active ingredient dominates the

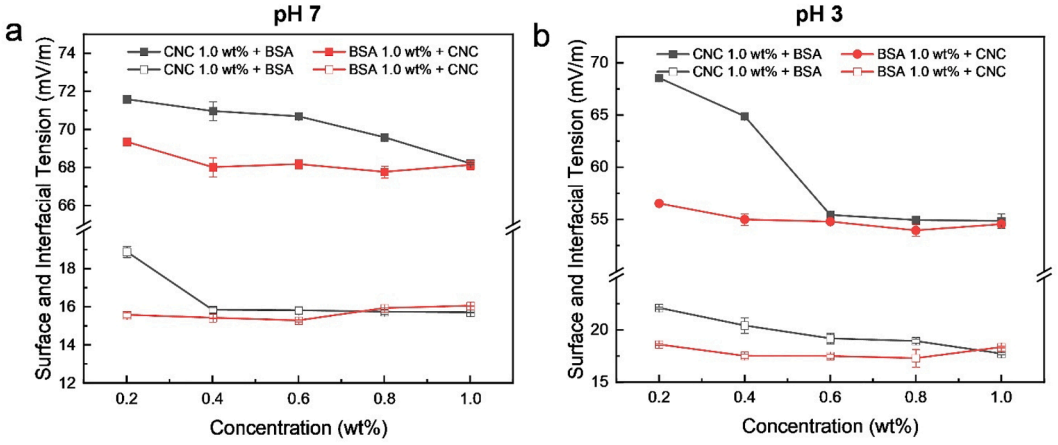

Fig. 3. Surface and interfacial tension of CNC/BSA mixtures at (a) pH 7 and (b) pH 3. Surface tension: filled symbol; interfacial tension: empty symbol.

interfacial behavior in the absence of strong interactions between the components. Similar trends in the surface tension and interfacial tension were observed at pH 3 despite the strong electrostatic interactions between these two oppositely charged compounds under such acidic conditions (Fig. 3b). When CNC was added to BSA solution, no obvious changes in both air/water surface tension and oil/water interfacial tension were observed upon increasing the concentration of the CNCs in the BSA solution.

In the case where BSA was added to a CNC dispersion, air/water surface tension rapidly decreased from 68.6 to 55.4 mN/m within a BSA concentrations range 0.2 to 0.6 wt%. The rapid drop in surface tension at pH 3 might be caused by the micellization of BSA on the surface of CNC particles. At oil/water interface, the interfacial tension decreased from 22.1 to 17.3 mN/m. This drop was also observed at pH 7, where the interfacial tension gradually reduced. This phenomenon demonstrates that electrostatic interactions are insufficient to counteract the surface activity of BSA.

3.4. Adsorption at solid surface

3.4.1. Monolayer adsorption of BSA

To explore the influence of pH on the layer-by-layer adsorption of BSA, measurements were initially performed by contacting the sensor surface with BSA solutions at pH 7 and pH 3. The adsorption properties of the samples were obtained by monitoring changes in the frequency (Δf) and dissipation shifts (ΔD) over time. As shown in Fig. 4a and 4b, a sudden drop in the frequency was observed, together with an increase in dissipation at both pH 7 and pH 3. These changes took place mainly during the initial pumping of BSA, suggesting a rapid adsorption process, and the decrease in frequency suggests mass adsorption on the surface of the sensor. Similar frequency variations were observed at both pH 7 and pH 3, indicating a similar adsorption of BSA at these two pH values; however, this does not necessarily indicate that the variation in the pH has no effect on BSA adsorption. Early results reported the adsorption of BSA has been reported to be higher at pH 5, and decreases were observed when the pH was reduced to 3 or increased to 7 (Jachimska, Tokarczyk, Łapczyńska, Puciul-Malinowska, & Zapotoczny, 2016). The calculated masses of BSA adsorbed under the various conditions were obtained using Eq. (1); these conditions are listed in Table S1. During the rinsing step, a small amount of weakly bound BSA was desorbed, giving final adsorbed masses of ~ 404.6 and 399.1 ng/cm^2 at pH 7 and pH 3, respectively. Furthermore, it was previously reported that dissipation values of $< 1 \times 10^{-6}$ were obtained for rigid surfaces (Mivehi, Bordes, & Holmberg, 2013), while in our case, the layer formed by BSA was rather viscoelastic ($\Delta D > 1 \times 10^{-6}$) at both pH 7 and pH 3 (Fig. 4a and b). Two factors may have contributed to this phenomenon. More specifically, the heterogeneous structure at the surface may cause the movement of the globular BSA proteins, while the protein layer can become highly hydrated at a pH value far from its pI to ultimately form a viscoelastic interconnected network (Corstens, Caltenco, de Vries, Schroën, & Berton-Carabin, 2017).

D-f plots, which represent the relationship between ΔD and Δf, eliminates the effect of time and is extensively employed to qualitatively illustrate the properties of an adsorbed layer. A lower $\Delta D/\Delta f$ value indicates a reduced amount of energy dissipation per frequency unit, which is characteristic of a rigid layer. Conversely, a higher $\Delta D/\Delta f$ value indicates a soft and viscoelastic layer (Zhang et al., 2020). Such *D-f* plots can also provide information regarding the adsorption kinetics, wherein a scatter curve represents 'fast' kinetics and a continuous curve represents 'slow' kinetics (Köhnke, Östlund, & Brelid, 2011). The adsorption process of each sample was therefore selected to draw the *D-f* curve and analyze the viscoelasticity of the adsorption layer. As shown in Fig. 4c, the *D-f* plot curves of BSA at both pH values changed gradually from scatter to continuous curves, indicating that the adsorption process shifted from fast to slow, and eventually reached equilibrium. A clear linear relationship can be observed in the *D-f* plots at pH 7, indicating that the adsorbed layer is always viscoelastic during adsorption. In contrast, the curve obtained at pH 3 showed that the adsorption process consisted of two clear stages, with a lower initial slope in the first stage and a sharply increasing slope in the second stage. This indicates that the adsorbed layer undergoes a transition from rigid to viscoelastic.

3.4.2. Sequential adsorption of BSA and the CNCs

Upon the formation of a steady BSA adsorption layer at the sensor surface after the rinsing step, the CNC suspension was introduced into the BSA layer prior to the final rinsing step. Fig. 5 shows the sequential adsorption of BSA and the CNCs at pH 7 and pH 3, wherein the same injection sequence was employed at both pH values. At pH 7, there was a slight increase in frequency (see Fig. 5a), indicating that there was no interaction between the CNCs and the adsorbed layer of BSA under neutral pH conditions. The final mass remained constant at ~ 241.5 ng/cm^2 (Table S1). This is due to the strong electrostatic repulsion between the anionic CNCs and the negatively charged BSA at pH values above their pI, as shown in Fig. 1b. Furthermore, an obvious increase in dissipation was evident following the introduction of the CNC suspension, which was likely due to a change in the properties of the bulk liquid caused by the higher viscosity of the CNC suspension compared to water (Kontturi, Tammelin, Johansson, & Stenius, 2008).

At pH 3, the addition of the CNC suspension resulted in a significant drop in the frequency (Fig. 5b), which suggested the occurrence of a second adsorption layer. After the final water flush to remove the loosely attached polymers, the frequency maintained a high value. The final mass absorbed remained at ~6840.6 ng/cm^2, which is significantly higher than the value before the introduction of the CNCs, thereby indicating that steady adsorption occurs because of electrostatic complexation. The dissipation also remained significantly higher than before, suggesting that CNC adsorption resulted in the formation of a more hydrated layer, which favored the generation of an electrostatic layer for stabilizing emulsions (Sarkar, Zhang, Murray, Russell, & Boxal, 2017). In terms of the *D-f* plots for the CNC adsorption process at pH 3 (Fig. 5c), the obtained curves indicate that the adsorption of the CNCs also underwent a process that changed from fast to slow adsorption.

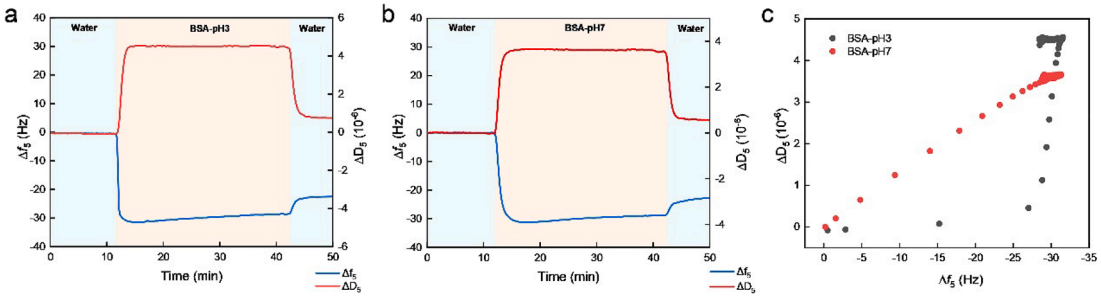

Fig. 4. Frequency (Δf) and dissipation (ΔD) shift at 5th overtone as a function of time for the adsorption of BSA at (a) pH 3 and (b) pH 7; (c) D-*f* plots for the adsorption process of BSA.

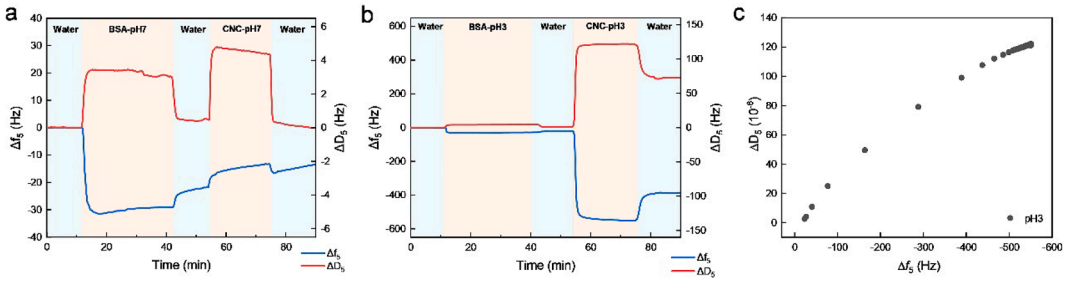

Fig. 5. Frequency (Δ*f*) and dissipation (ΔD) shift at 5th overtone as a function of time for the sequential adsorption of BSA and then CNC at (a) pH 7 and (b) pH 3. D-*f* plots during CNC adsorption.

Overall, these results further confirm the formation of electrostatic CNC/BSA complexes at pH 3. Based on these results, it can also be predicted that at pH 3, the stability of the oil droplets in the CNC/BSA-stabilized emulsions were superior to those at pH 7. As a result, at pH 3, the oil droplets present in the emulsion will possess a thicker and more viscoelastic layer to protect them from destabilization. Comparable findings have been reported for the successive adsorption of other proteins and polysaccharides. Bertsch, Thoma, Bergfreund, Geue, and Fischer (2019) investigated the successive adsorption of β-lactoglobulin (β-lg) and low-methoxyl pectin at pH 4 using an interfacial shear rheology setup. Their work pointed out that successive adsorption of pectin increased the viscoelasticity of an adsorbed β-lg layer by electrostatic complexation. The successive adsorption demonstrates outstanding advantages in improving the interfacial viscoelasticity compared to simultaneous adsorption or directly complexing polysaccharides and proteins in the bulk phase prior to adsorption (Ganzevles, Stuart, van Vliet, & de Jongh, 2006; Ramamirtham, Williams, Zare, Weeks, & Whitby, 2021).

In emulsions formed by sequential adsorption of protein and polysaccharide, also known as layer-by-layer emulsions, the existence of the secondary polysaccharide layer could also provide steric repulsion and prevent hydrolysis during digestion. A previous study investigating CNC and β-lactoglobulin protein interfacial layers revealed that CNC serves as a steric barrier for pepsin and may improve the stability in a gastric environment when there is sufficient CNC (Scheuble, Geue, Windhab, & Fischer, 2014). Similar anti-digestibility performance was also reported in cellulose nanofiber by protecting the inner phase from digestive enzymes (Zhang et al., 2019).

3.5. MD simulations

To gain further insights into the interaction mechanism between single CNCs and BSA, MD simulations were conducted. Fig. 6a shows the crystal structure of the CNCs, wherein two surfaces with different hydrophilic capabilities were considered (100 and 110). The (1 0 0) surface displayed a hydrophobic character because of less exposed –OH groups and the lower surface roughness, whereas the (1 1 0) surface possessed a higher surface roughness and exhibited hydrophilic features (Ma et al.,

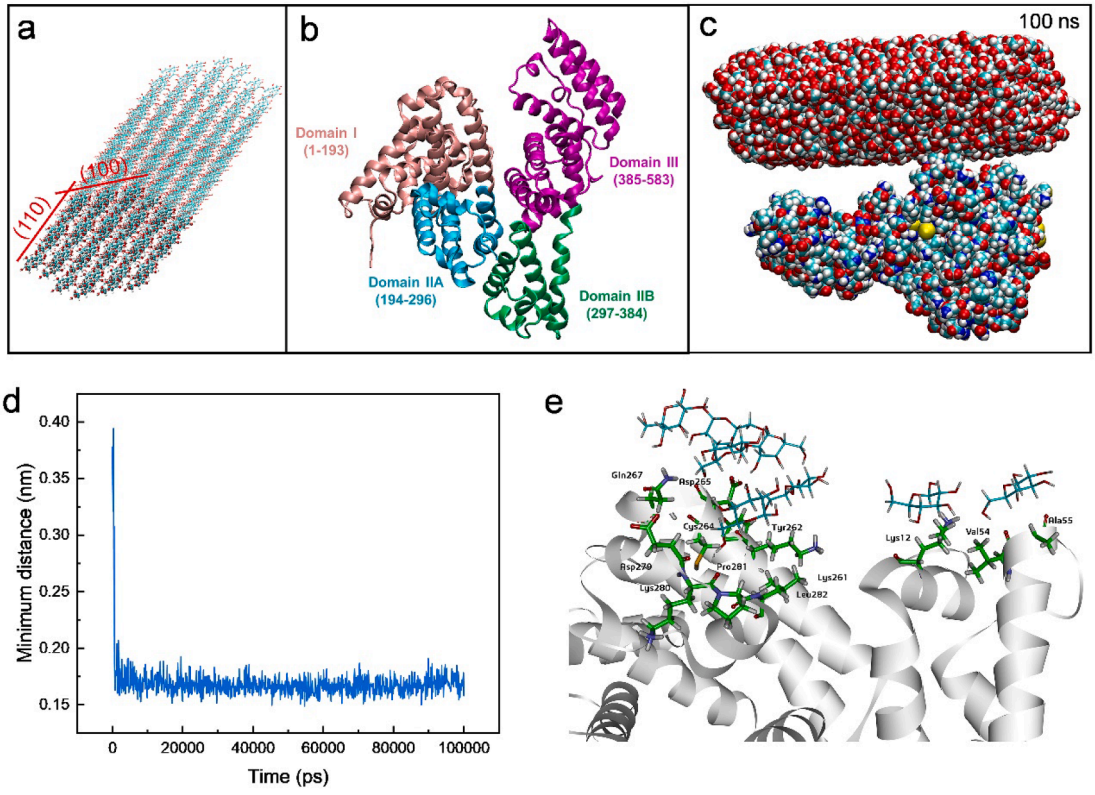

Fig. 6. (a) Side view of the CNC. (b) Cartoon structure of BSA. (c) Snapshots at the end of the simulation of CNC and BSA interaction (100 ns), all the water molecules were deleted to highlight CNC and BSA. (d) Plot of minimum distance between CNC and BSA versus simulation time. (e) Interaction sites of CNC and BSA.

2021). Such heterogeneity in the different surfaces of CNCs is important in terms of its interactions with proteins since the protein may approach different areas of the CNC surface. In addition, Fig. 6b shows the structure of BSA, which is composed of 583 amino acids and is divided into three domains, namely, domain I (1–193), domain II (194–384), and domain III (385–583). Each domain comprises subdomains A and B, among which IIA (194–296) and IIIA (385–497) are common active sites (Lv et al., 2021). The results of the MD simulations showed that BSA is more prone to interact with the (1 0 0) surface of the CNCs (Fig. 6c). The time evolution of the minimum distance was then calculated to confirm the existence of interactions between BSA and the CNCs, and it was found that BSA rapidly contacts with the CNCs during a short equilibration run of 600 ps and remains adsorbed until the end of the simulation (see Fig. 6d). The contact between BSA and the CNCs mainly occurs through the domain IIA region of BSA, which is composed of the Lys261, Tyr262, Cys264, Asp265, Gln267, Asp 279, Lys280, Pro281, and Leu282 amino acid residues (Fig. 6e). In addition to these residues, BSA possesses Lys12, Val54, and Ala55 residues, which are adsorbed on the CNC surface. These results suggest that the substantial interactions between the CNCs and BSA are mostly produced between the hydrophobic surfaces of the CNCs and the domain IIA region of BSA.

4. Conclusion

Combinational interfacial approaches and QCM-D were used to explore the interactions between CNC and BSA at both pH 7 and pH 3. Interfacial measurements carried out for the air/water and oil/water interfaces confirmed the surface activity of BSA under different environmental conditions (pH, concentration, and mixing ratio), which provided the dominant surface activity in a complex CNC–protein system. The QCM-D results revealed that the sequential adsorption of BSA and the CNCs tended to lead to the formation of a soft and viscoelastic bilayer at pH 3, and the mass adsorbed was significantly higher than that observed for BSA alone, thereby indicating the potential of this system in the steric stabilization of emulsions. The different interactions, including the varying interfacial activities and interfacial adsorption properties between the CNCs and the negatively and positively charged BSA at different pH values confirmed the critical role of pH in modulating the interactions between these species. Furthermore, MD simulations provided an understanding of these interactions in the context of the BSA active sites and the heterogeneity of the different CNC crystal planes. Overall, considering the current trend in the design of bio-based composite particles, this work can provide quantitative insights into the interactions between cellulose-based particles and proteins, which is useful for illustrating the interfacial stabilization mechanisms in complex food colloidal systems.

CRediT authorship contribution statement

Xinna Hu: Conceptualization, Investigation, Methodology, Writing – original draft. **Tao Ma:** Formal analysis, Software, Validation, Writing – review & editing. **Shuyu Lu:** Validation, Project administration. **Yi Song:** Supervision, Funding acquisition, Writing – review & editing.

Declaration of Competing Interest

The authors declare that they have no known competing financial interests or personal relationships that could have appeared to influence the work reported in this paper.

Acknowledgments

The work was supported by the National Natural Science Foundation of China (No. 31871814), and the 2115 Talent Development Program of China Agricultural University. We also highly appreciate the support from China Scholarship Council for Xinna Hu.

Appendix A. Supplementary data

Supplementary data to this article can be found online at https://doi.org/10.1016/j.fochx.2021.100194.

References

Bergfreund, J., Sun, Q., Fischer, P., & Bertsch, P. (2019). Adsorption of charged anisotropic nanoparticles at oil–water interfaces. *Nanoscale Advances, 1*(11), 4308–4312. https://doi.org/10.1039/C9NA00506D

Bertsch, P., Diener, M., Adamcik, J., Scheuble, N., Geue, T., Mezzenga, R., & Fischer, P. (2018). Adsorption and interfacial layer structure of unmodified nanocrystalline cellulose at air/water interfaces. *Langmuir, 34*(50), 15195–15202. https://doi.org/10.1021/acs.langmuir.8b03056

Bertsch, P., Thoma, A., Bergfreund, J., Geue, T., & Fischer, P. (2019). Transient measurement and structure analysis of protein–polysaccharide multilayers at fluid interfaces. *Soft Matter, 15*(31), 6362–6368. https://doi.org/10.1039/c9sm01112a

Chen, Q., Xu, S., Liu, Q., Masliyah, J., & Xu, Z. (2016). QCM-D study of nanoparticle interactions. *Advances in Colloid and Interface Science, 233*, 94–114. https://doi.org/10.1016/j.cis.2015.10.004

Corstens, M. N., Caltenco, L. A. O., de Vries, R., Schroën, K., & Berton-Carabin, C. C. (2017). Interfacial behaviour of biopolymer multilayers: Influence of in vitro digestive conditions. *Colloids and Surfaces B: Biointerfaces, 153*, 199–207. https://doi.org/10.1016/j.colsurfb.2017.02.019

Derkach, S. R., Voron'ko, N. G., Sokolan, N. I., Kolotova, D. S., & Kuchina, Y. A. (2020). Interactions between gelatin and sodium alginate: UV and FTIR studies. *Journal of Dispersion Science and Technology, 41*(5), 690–698. https://doi.org/10.1080/01932691.2019.1611437

Ganzevles, R. A., Stuart, M. A. C., van Vliet, T., & de Jongh, H. H. (2006). Use of polysaccharides to control protein adsorption to the air–water interface. *Food Hydrocolloids, 20*(6), 872–878. https://doi.org/10.1016/j.foodhyd.2005.08.009

Gomes, T. C. F., & Skaf, M. S. (2012). Cellulose-Builder: A toolkit for building crystalline structures of cellulose. *Journal of Computational Chemistry, 33*(14), 1338–1346. https://doi.org/10.1002/jcc.v33.1410.1002/jcc.22959

Jachimska, B., Tokarczyk, K., Łapczyńska, M., Puciul-Malinowska, A., & Zapotoczny, S. (2016). Structure of bovine serum albumin adsorbed on silica investigated by quartz crystal microbalance. *Colloids and Surfaces A: Physicochemical and Engineering Aspects, 489*, 163–172. https://doi.org/10.1016/j.colsurfa.2015.10.033

Köhnke, T., Östlund, Å., & Brelid, H. (2011). Adsorption of arabinoxylan on cellulosic surfaces: Influence of degree of substitution and substitution pattern on adsorption characteristics. *Biomacromolecules, 12*(7), 2633–2641. https://doi.org/10.1021/bm200437m

Kontturi, K. S., Tammelin, T., Johansson, L.-S., & Stenius, P. (2008). Adsorption of cationic starch on cellulose studied by QCM-D. *Langmuir, 24*(9), 4743–4749. https://doi.org/10.1021/la703604j

Lee, H.-S., Myers, C., Zaidel, L., Nalam, P. C., Caporizzo, M. A., Daep, C. A., Eckmann, D. M., Masters, J. G., & Composto, R. J. (2017). Competitive adsorption of polyelectrolytes onto and into pellicle-coated hydroxyapatite investigated by QCM-D and force spectroscopy. *ACS Applied Materials & Interfaces, 9*(15), 13079–13091. https://doi.org/10.1021/acsami.7b0277410.1021/acsami.7b02774.s001

Li, M., McClements, D. J., Liu, X., & Liu, F. (2020). Design principles of oil-in-water emulsions with functionalized interfaces: Mixed, multilayer, and covalent complex structures. *Comprehensive Reviews in Food Science and Food Safety, 19*(6), 3159–3190. https://doi.org/10.1111/1541-4337.12622

Li, H., Wang, D., Liu, C., Zhu, J., Fan, M., Sun, X., Wang, T., Xu, Y., & Cao, Y. (2019). Fabrication of stable zein nanoparticles coated with soluble soybean polysaccharide for encapsulation of quercetin. *Food Hydrocolloids, 87*, 342–351. https://doi.org/10.1016/j.foodhyd.2018.08.002

Li, H., Wu, J., Doost, A. S., Su, J., & Van der Meeren, P. (2021). Electrostatic interaction between whey proteins and low methoxy pectin studied by quartz crystal microbalance with dissipation monitoring. *Food Hydrocolloids, 113*, 106489. https://doi.org/10.1016/j.foodhyd.2020.106489

Liu, X., Shi, S., Li, Y., Forth, J., Wang, D., & Russell, T. P. (2017). Liquid tubule formation and stabilization using cellulose nanocrystal surfactants. *Angewandte Chemie, 129*(41), 12768–12772. https://doi.org/10.1002/ange.201706839

Liu, F., Zheng, J., Huang, C.-H., Tang, C.-H., & Ou, S.-Y. (2018). Pickering high internal phase emulsions stabilized by protein-covered cellulose nanocrystals. *Food Hydrocolloids, 82*, 96–105. https://doi.org/10.1016/j.foodhyd.2018.03.047

Lozeau, L. D., Rolle, M. W., & Camesano, T. A. (2018). A QCM-D study of the concentration-and time-dependent interactions of human LL37 with model mammalian lipid bilayers. *Colloids and Surfaces B: Biointerfaces, 167*, 229–238. https://doi.org/10.1016/j.colsurfb.2018.04.016

Lv, Y., Liang, Q., Li, Y., Liu, X., Zhang, D., & Li, X. (2021). Study of the binding mechanism between hydroxytyrosol and bovine serum albumin using multispectral and molecular docking. *Food Hydrocolloids, 122*, 107072. https://doi.org/10.1016/j.foodhyd.2021.107072

Ma, T., Hu, X., Lu, S., Cui, R., Zhao, J., Hu, X., & Song, Y. (2021). Cellulose nanocrystals produced using recyclable sulfuric acid as hydrolysis media and their wetting molecular dynamics simulation. *International Journal of Biological Macromolecules, 184*, 405–414. https://doi.org/10.1016/j.ijbiomac.2021.06.094

Ma, T., Hu, X., Lu, S., Liao, X., Song, Y., & Hu, X. (2020). Nanocellulose: A promising green treasure from food wastes to available food materials. *Critical Reviews in Food Science and Nutrition*. https://doi.org/10.1080/10408398.2020.1832440

Mikulcová, V., Bordes, R., Minařík, A., & Kašpárková, V. (2018). Pickering oil-in-water emulsions stabilized by carboxylated cellulose nanocrystals–Effect of the pH. *Food Hydrocolloids, 80*, 60–67. https://doi.org/10.1016/j.foodhyd.2018.01.034

Mivehi, L., Bordes, R., & Holmberg, K. (2013). Adsorption of cationic gemini surfactants at solid surfaces studied by QCM-D and SPR—Effect of the presence of hydroxyl groups in the spacer. *Colloids and Surfaces A: Physicochemical and Engineering Aspects, 419*, 21–27. https://doi.org/10.1016/j.colsurfa.2012.11.044

Nguyen, P. N., Waton, G., Vandamme, T., & Krafft, M. P. (2013). Reversing the course of the competitive adsorption between a phospholipid and albumin at an air–water interface. *Soft Matter, 9*(42), 9972–9976. https://doi.org/10.1039/C3SM51941D

Pathak, J., Priyadarshini, E., Rawat, K., & Bohidar, H. B. (2017). Complex coacervation in charge complementary biopolymers: Electrostatic versus surface patch binding. *Advances in Colloid and Interface Science, 250*, 40–53. https://doi.org/10.1016/j.cis.2017.10.006

Peters, T., Jr (1995). *All about albumin: Biochemistry, genetics, and medical applications.* Academic press.

Ramamirtham, S., Williams, M. A., Zare, D., Weeks, M., & Whitby, C. P. (2021). Complexes of β-lactoglobulin and high methyl-esterified pectin as a one-shot delivery system for reinforcing oil/water interfaces. *Soft Matter, 17*(37), 8517–8522. https://doi.org/10.1039/D1SM00989C

Richardson, J. J., Cui, J., Björnmalm, M., Braunger, J. A., Ejima, H., & Caruso, F. (2016). Innovation in layer-by-layer assembly. *Chemical Reviews, 116*(23), 14828–14867. https://doi.org/10.1021/acs.chemrev.6b00627

Sarkar, A., Li, H., Cray, D., & Boxall, S. (2018). Composite whey protein–cellulose nanocrystals at oil-water interface: Towards delaying lipid digestion. *Food Hydrocolloids, 77*, 436–444. https://doi.org/10.1016/j.foodhyd.2017.10.020

Sarkar, A., Zhang, S., Holmes, M., & Ettelaie, R. (2019). Colloidal aspects of digestion of Pickering emulsions: Experiments and theoretical models of lipid digestion kinetics. *Advances in Colloid and Interface Science, 263*, 195–211. https://doi.org/10.1016/j.cis.2018.10.002

Sarkar, A., Zhang, S., Murray, B., Russell, J. A., & Boxal, S. (2017). Modulating in vitro gastric digestion of emulsions using composite whey protein-cellulose nanocrystal interfaces. *Colloids and Surfaces B: Biointerfaces, 158*, 137–146. https://doi.org/10.1016/j.colsurfb.2017.06.037

Sauerbrey, G. (1959). The use of quarts oscillators for weighing thin layers and for microweighing. *Z. Phys., 155*, 206–222. https://doi.org/10.1007/BF01337937

Scheuble, N., Geue, T., Windhab, E. J., & Fischer, P. (2014). Tailored interfacial rheology for gastric stable adsorption layers. *Biomacromolecules, 15*(8), 3139–3145. https://doi.org/10.1021/bm500767c

Urbánková, L., Sedláček, T., Kašpárková, V., & Bordes, R. (2021). Formation of oleogels based on emulsions stabilized with cellulose nanocrystals and sodium caseinate. *Journal of Colloid and Interface Science, 596*, 245–256. https://doi.org/10.1016/j.jcis.2021.02.104

Van Der Spoel, D., Lindahl, E., Hess, B., Groenhof, G., Mark, A. E., & Berendsen, H. J. C. (2005). GROMACS: Fast, flexible, and free. *Journal of Computational Chemistry, 26*(16), 1701–1718. https://doi.org/10.1002/(ISSN)1096-987X10.1002/jcc.v26:1610.1002/jcc.20291

Wei, Y., Guo, A., Liu, Z., Mao, L., Yuan, F., Gao, Y., & Mackie, A. (2021). Structural design of zein-cellulose nanocrystals core–shell microparticles for delivery of curcumin. *Food Chemistry, 357*, 129849. https://doi.org/10.1016/j.foodchem.2021.129849

Wijaya, W., Patel, A. R., Setiowati, A. D., & Van der Meeren, P. (2017). Functional colloids from proteins and polysaccharides for food applications. *Trends in Food Science & Technology, 68*, 56–69. https://doi.org/10.1016/j.tifs.2017.08.003

Wu, X., Yuan, Q., Liu, S., Shi, S., Russell, T. P., & Wang, D. (2019). Nanorod–surfactant assemblies and their interfacial behavior at liquid–liquid interfaces. *ACS Macro Letters, 8*(5), 512–518. https://doi.org/10.1021/acsmacrolett.9b00134

Zhang, X., Liu, Y., Wang, Y., Luo, X., Li, Y., Li, B., … Liu, S. (2019). Surface modification of cellulose nanofibrils with protein nanoparticles for enhancing the stabilization of O/W pickering emulsions. *Food Hydrocolloids, 97*, 105180. https://doi.org/10.1016/j.foodhyd.2019.105180

Zhang, J., Mei, L., Chen, N., Yuan, Y., Zeng, Q.-Z., & Wang, Q. (2020). Study on β-lactoglobulin microgels adsorption onto a hydrophobic solid surface by QCM-D. *Food Hydrocolloids, 98*, 105320. https://doi.org/10.1016/j.foodhyd.2019.105320